

Research



Cite this article: Erdle H, Böhlke T. 2023

Analytical investigation of a grain boundary model that accounts for slip system coupling in gradient crystal plasticity frameworks. *Proc. R. Soc. A* **479**: 20220737.

<https://doi.org/10.1098/rspa.2022.0737>

Received: 4 November 2022

Accepted: 20 April 2023

Subject Areas:

mechanical engineering, materials science, computational mechanics

Keywords:

crystal plasticity, gradient plasticity, extended continuum, grain boundary model, slip system coupling

Authors for correspondence:

H. Erdle

e-mail: hannes.erdle@kit.edu

T. Böhlke

e-mail: thomas.boehlke@kit.edu

Electronic supplementary material is available online at <https://doi.org/10.6084/m9.figshare.c.6631533>.

Analytical investigation of a grain boundary model that accounts for slip system coupling in gradient crystal plasticity frameworks

H. Erdle and T. Böhlke

Institute of Engineering Mechanics, Chair for Continuum Mechanics, Karlsruhe Institute of Technology (KIT), Kaiserstrasse 12, 76131 Karlsruhe, Germany

HE, 0000-0002-1898-6272

In this work, a physically based dislocation theory of plasticity is derived within an extended continuum mechanical context. An orientation-dependent grain boundary flow rule is introduced for the modelling of dislocation pile-up at grain boundaries and dislocation transmission through grain boundaries. With the conventional grain boundary modelling approach according to Gurtin (Gurtin. 2008 *J. Mech. Phys. Solids* **56**, 640–662. (doi:10.1016/j.jmps.2007.05.002)) the single-crystal consistency check for the limit case of adjacent grains that hold no misorientation is not satisfied. In order to overcome this modelling shortcoming, a slip system coupling based on a geometric measure of slip system compatibility is introduced. In order to investigate the grain boundary modelling approaches, the analytical solution of a three-phase periodic laminate is used to study the interactions of dislocations and grain boundaries within the gradient crystal plasticity framework. With the developed grain boundary model two grain boundary states, i.e. microhard and microcontrolled, are observed for misaligned grains. This allows the modelling of slip activation at grain boundaries based on the dislocation pile-up stress.

1. Introduction

In early work on gradient plasticity, grain boundaries act as insurmountable barriers to plastic slip [1]. In such

a microhard state, no plastic deformation occurs within the grain boundaries. In contrast to this assumption, the microfree grain boundary condition implies that the grain boundaries allow free dislocation transmission. In Gurtin & Needleman [2], microhard and microfree boundary conditions are discussed in the context of gradient crystal plasticity. In order to model grain boundary behaviour between these limit cases, slip transmission criteria must be introduced.

Experimentally, the grain boundary slip transmission can be investigated, e.g. by nanoindentation. Hereby, the mechanical response to nanoindentation is recorded as a function of distance to the grain boundary, cf. e.g. [3,4]. In Soer *et al.* [5], a displacement jump is observed during the indentation of a nano-indenter close to a grain boundary. In Wang & Ngan [6], it is shown that this so-called grain boundary pop-in effect is closely related to the misorientation between slip systems at the grain boundary. The orientation-dependent tendency of this behaviour is confirmed by Wo & Ngan [7]. The characterization is severely limited by the instrumented indentation and recording resolution. Recent works address these issues and obtain advances by automation of measurement and data analysis [8]. In addition to nanoindentation, *in situ* electron microscope measurements and diffraction contrast electron tomography can be used to investigate work hardening effects of dislocations [9], or dislocation-grain boundary interactions [10]. With multiple dislocation systems being active simultaneously, however, the investigation of dislocation-grain boundary interactions is complex. Models and simulations of grain boundary slip transmission are needed to better understand the dislocation-grain boundary interactions in polycrystalline materials.

Modelling approaches of grain boundaries can be categorized into continuum defect models, diffuse interface models and sharp interface models, cf. the review article of Clayton [11]. In the early work of Read & Shockley [12], a continuum dislocation model of low-angle grain boundaries is constructed. The resulting grain boundary energy strongly depends on the relative rotation of adjacent grains. In order to account for larger misorientation angles of high-angle grain boundaries, Wolf [13] generalizes the Read–Shockley expression of the grain boundary energy. Diffuse interface models treat grain boundaries as regions of finite width, defined through the evolution of so-called phase fields. This allows the description of moving grain boundaries kinetics, cf. e.g. the phase field—crystal plasticity coupling of Abrivard *et al.* [14]. In this work, sharp interface models are considered, in which properties of crystals in the immediate vicinity of the boundary are identical to those far from the interface. With the sharp interface representation, the discontinuity and the transition of field variables, e.g. slip, across interfaces can be considered. For an overview of slip transmission criteria within the simulations of polycrystalline materials based on sharp interface models, the reader is referred to the review article of Bayerschen *et al.* [15]. Some examples include dislocation density-based formulae for crystalline plasticity [16], a modification of the classical crystal plasticity model in which slip transmission is allowed only for small-angle boundaries [17], or atomistic simulations [18]. The geometric criteria for slip transmission have in common that the transmission of dislocations occurs predominantly at low-angle grain boundaries. In Liu *et al.* [19], it is shown that dislocation source activation occurs at high-angle grain boundaries. This effect, however, is not considered in this work.

This work investigates the extrinsic grain boundary dislocation energy of Gurtin [20], which depends on Nye's dislocation density tensor [21]. The extrinsic grain boundary dislocation energy accounts for the misorientation of slip systems between adjacent grains. The modelling of the intra-grain and inter-grain dislocation interactions on different slip systems provides a physically meaningful basis for polycrystalline structures. The pile-up of dislocations at the grain boundaries and the transmission across the grain boundaries depends only on the corresponding extrinsic grain boundary dislocation energy. This energy is formulated as a function of the left-hand limits and right-hand limits of plastic slips at the grain boundaries. The common approach for the grain boundary modelling is based on the assumption of independent plastic slip rates at the grain boundaries. As shown in this work, this assumption leads to artefacts of slip distributions across grain boundaries for the limit case of two adjacent grains that hold no misorientation. For this limit case of equally orientated grains, and under the assumption of identical material properties, the grain boundary should not be observable. The slip distribution that results

from the assumption of independent plastic slip rates, however, is discontinuous across the non-existing boundary. In order to overcome this modelling shortcoming, a new approach of coupled slip systems at grain boundaries is introduced. Peng *et al.* [22] couple the plastic slips for the incoming slip systems with the outgoing slip systems using kinematic relations under the assumption of continuous plastic slip distributions across grain boundaries. In this work, the general case of a discontinuous plastic slip distribution is considered. An additional grain boundary flow rule is introduced based on the discontinuity of the plastic slip gradient. The coupling of slip systems at the grain boundaries is formulated based on the geometric condition of Werner & Prantl [23], thereby accounting for the dislocation transmission dependent on the misorientation of slip systems. In Hamid *et al.* [24], a coupled grain boundary model is constructed in a continuum dislocation dynamics framework. For each pair of slip systems, a slip transmission coefficient, as introduced in Werner & Prantl [23], is calculated based on the angle between slip planes and the angle between slip directions. The grain boundary strength is assumed as a linear function of the slip transmission coefficient. Alipour *et al.* [25] formulate a grain boundary model based on the geometric condition of Werner & Prantl [23] in a gradient-extended framework. Hereby, an overall slip transmission coefficient is constructed based on all combinations of slip systems. In contrast to Hamid *et al.* [24], the assumed dependency of the grain boundary yield strength is able to predict the limiting case of a microhard grain boundary. Additionally to the limiting case of a microhard grain boundary for strongly misaligned grains, the grain boundary modelling approach presented in this work passes the single-crystal consistency check for the limit case of equally orientated slip systems at grain boundaries.

In addition to the single-crystal consistency check the influence of a varying grain misorientation is investigated. With the presented grain boundary modelling approach misaligned grains at first behave microhard, i.e. no slip transmission across the grain boundary occurs, until a critical state is reached. This is consistent with the experimental observations of Sun *et al.* [26], where the distribution of dislocations within an aluminium bicrystal is investigated. At lower strains, a pile-up of dislocations near the grain boundary is observed, which is flattened at a higher strain. Whereas the common approach for grain boundary modelling is not able to predict this behaviour, the presented approach accounts for the activation of grain boundary slip by introducing a critical pileup stress, which depends on the misorientation angle between slip systems of adjacent grains. Consequently, the presented model is able to predict an orientation-dependent grain boundary behaviour, while accounting for the limits of a microfree grain boundary behaviour for equally orientated grains and a microhard grain boundary behaviour for strongly misaligned grains.

In this work, in order to investigate grain boundary slip transmission by an analytical solution, a gradient crystal plasticity framework is applied to the shearing of a three-phase periodic laminate structure for the special case of a single slip. A similar problem, i.e. the shearing of a two-phase laminate structure consisting of an elasto-plastic phase and an elastic phase, has been studied in Sedláček & Forest [27]. Forest & Sedláček [28] consider the boundary value problem in order to compare dislocation-based, Cosserat and strain-gradient models of crystal plasticity. In Forest [29], the extension to a cyclic deformation is made to investigate kinematic hardening. Further applications to two-phase laminate have been made in Cordero *et al.* [30] and Aslan *et al.* [31] to study size effects, as well as in Forest & Guéninchault [32] and Wulfinghoff *et al.* [33] to study free energy potentials in gradient crystal plasticity. Erdle & Böhlke [34] consider a two-phase laminate consisting of two elasto-plastic phases to study grain boundary effects within gradient crystal plasticity. Prahs & Böhlke [35] consider a three-phase laminate structure to study the influence of material parameters of the grain boundary modelling approach of Gurtin [20]. Hereby, however, the special case of coherent slip systems orthogonal to the grain boundaries is considered, whereas in this work the influence of the orientation of slip systems and orientation of grain boundaries on the transmission of slip is studied.

Notation: Vectors are denoted by lowercase letters in boldface, e.g. \mathbf{a} , whereas tensors are denoted by uppercase letters in boldface, e.g. \mathbf{A} . The dot product between two vectors is defined

by $\mathbf{a} \cdot \mathbf{b} = |\mathbf{a}||\mathbf{b}| \cos(\angle(\mathbf{a}, \mathbf{b}))$ and for tensors $\mathbf{A} \cdot \mathbf{B} = \text{tr}(\mathbf{A}^T \mathbf{B})$. The outer product is defined by $(\mathbf{u} \otimes \mathbf{v})\mathbf{a} = (\mathbf{v} \cdot \mathbf{a})\mathbf{u}$. The cross product is defined by $\mathbf{a} \times \mathbf{b} = a_i b_j \epsilon_{ijk} \mathbf{e}_k$, where $\epsilon = \epsilon_{ijk} \mathbf{e}_i \otimes \mathbf{e}_j \otimes \mathbf{e}_k$ with $i, j, k \in \{1, 2, 3\}$ denotes the permutation tensor and $\{\mathbf{e}_1, \mathbf{e}_2, \mathbf{e}_3\}$ is an orthonormal basis. Moreover, $\mathbf{t} = \boldsymbol{\sigma} \mathbf{n}$ denotes the linear mapping $\mathbf{n} \mapsto \mathbf{t}$ obtained by the multiplication between the second-order tensor $\boldsymbol{\sigma}$ with a first-order tensor \mathbf{n} . Similarly, $\boldsymbol{\sigma} = \mathbb{C}[\boldsymbol{\epsilon}_e]$ denotes the linear mapping $\boldsymbol{\epsilon}_e \mapsto \boldsymbol{\sigma}$, where \mathbb{C} is a fourth-order tensor and $\boldsymbol{\epsilon}_e$ a second-order tensor. The jump $\{\mathbf{a}\} = \mathbf{a}^+ - \mathbf{a}^-$ and mean value $\langle \mathbf{a} \rangle = (\mathbf{a}^+ + \mathbf{a}^-)/2$ of an arbitrary vector field \mathbf{a} are defined at a singular surface, where \mathbf{a}^+ and \mathbf{a}^- denote the right-hand limit and left-hand limit of \mathbf{a} at the singular surface, respectively.

2. Gradient crystal plasticity framework

(a) Kinematics and basic assumptions

Under the assumption of small deformations, i.e. $\|\text{grad}(\mathbf{u})\| \ll 1$, the infinitesimal strain $\boldsymbol{\epsilon} = \text{sym}(\text{grad}(\mathbf{u}))$ is assumed to be additively decomposed into an elastic part $\boldsymbol{\epsilon}_{el}$ and a plastic part $\boldsymbol{\epsilon}_p$, i.e. $\boldsymbol{\epsilon} = \boldsymbol{\epsilon}_{el} + \boldsymbol{\epsilon}_p$. The general linear elastic anisotropic material law $\boldsymbol{\sigma} = \mathbb{C}[\boldsymbol{\epsilon}_e]$ connects the Cauchy stress tensor $\boldsymbol{\sigma}$ and elastic strains $\boldsymbol{\epsilon}_{el}$ by a linear relationship. The plastic strain rate tensor

$$\dot{\boldsymbol{\epsilon}}_p = \sum_{\alpha=1}^N \dot{\gamma}_\alpha \mathbf{M}_\alpha^s, \quad (2.1)$$

is modelled by classical crystal plasticity superimposing slip rates $\dot{\gamma}_\alpha$ on the individual slip systems, where $\alpha \in \{1, \dots, N\}$ denotes the slip indices and N is the number of slip systems. For simplicity, following the work of Gurtin [20], it is assumed that the number of slip systems is constant within the material. Each slip system is characterized by the corresponding symmetric part of the Schmid tensor $\mathbf{M}_\alpha^s = \text{sym}(\mathbf{d}_\alpha \otimes \mathbf{n}_\alpha)$, with the slip plane normal vector \mathbf{n}_α and the slip direction \mathbf{d}_α . For each slip system, the accumulated plastic slip

$$\gamma_{\alpha c} = \int |\dot{\gamma}_\alpha| dt, \quad (2.2)$$

is introduced as an internal hardening variable. Note that the accumulated plastic slip is not a directly observable quantity. Based on a phenomenological approach, evolution equations for the dislocation densities can be constructed, e.g. by the Kocks–Mecking relation [36,37]. This allows the calibration of a limited set of parameters by experiments and a computationally more efficient modelling. For a model approach, which is based on densities of dislocations, the reader is referred to the thermodynamic dislocation theory of Le [38] and the accompanying work on dislocation-grain boundary interactions of Piao & Le [39].

(b) Principle of virtual power

In the following, local field equations are obtained for each slip system based on the principle of virtual power. The microscopic and macroscopic force systems of the polycrystalline body are introduced in Cermelli & Gurtin [40]. For the bulk material, additionally to the Cauchy stress tensor $\boldsymbol{\sigma}$ that expends power over the elastic strain rate $\dot{\boldsymbol{\epsilon}}_e$, Cermelli & Gurtin [40] define for each slip system α a scalar-valued microscopic stress π_α that expends power over the slip rates $\dot{\gamma}_\alpha$ and a vector-valued microscopic stress $\boldsymbol{\xi}_\alpha$ that expends power over the slip rate gradients $\text{grad}(\dot{\gamma}_\alpha)$ are introduced. For the grain boundaries, the microtractions Π_α^+ and Π_α^- are introduced, which expend power over the right-hand limit and left-hand limit of the slip rates $\dot{\gamma}_\alpha^+$ and $\dot{\gamma}_\alpha^-$, respectively. Motivated by the framework of Gurtin & Needleman [2], the grain boundary contributions are introduced in a form $\{\Pi_\alpha \dot{\gamma}_\alpha\}$. Please note that, due to the nature of the slip systems and the corresponding slips γ_α , no continuity condition can be defined for the slips γ_α^+ , γ_α^- on a grain boundary. In this work, cavitation at the grain boundaries and grain boundary slip are not taken into account, i.e. $\{\mathbf{u}\} = \mathbf{0}$. Based on the individual contributions the internal power

is given as

$$\mathcal{P}_{\text{int}} = \int_{\mathcal{V}} \left(\boldsymbol{\sigma} \cdot \dot{\boldsymbol{\epsilon}}_e + \sum_{\alpha=1}^N (\pi_{\alpha} \dot{\gamma}_{\alpha} + \boldsymbol{\xi}_{\alpha} \cdot \text{grad}(\dot{\gamma}_{\alpha})) \right) dv + \int_S \sum_{\alpha=1}^N \{ \Pi_{\alpha} \dot{\gamma}_{\alpha} \} da. \quad (2.3)$$

The contributions to the power of external forces are chosen based on the work of Gurtin [1]. The macroscopic system is defined by a body force density $\rho \mathbf{b}$ and a surface traction $\bar{\mathbf{t}}$, both associated with $\dot{\mathbf{u}}$. Additionally, for each slip system α , a microscopic surface traction $\bar{\Pi}_{\alpha}$ is defined, which is associated with the plastic slip rate $\dot{\gamma}_{\alpha}$. Consequently, the power of external forces is given as

$$\mathcal{P}_{\text{ext}} = \int_{\mathcal{V}} \rho \mathbf{b} \cdot \dot{\mathbf{u}} dv + \int_{\partial \mathcal{V}_t} \bar{\mathbf{t}} \cdot \dot{\mathbf{u}} da + \int_{\partial \mathcal{V}_{\Pi}} \sum_{\alpha=1}^N \bar{\Pi}_{\alpha} \dot{\gamma}_{\alpha} da, \quad (2.4)$$

where $\partial \mathcal{V}_t$ denotes the Neumann boundary corresponding to $\bar{\mathbf{t}}$ and $\partial \mathcal{V}_{\Pi}$ denotes the Neumann boundary corresponding to $\bar{\Pi}$.

The principle of virtual power states that for all generalized virtual velocities the internal and external virtual powers are balanced, i.e.

$$\delta \mathcal{P}_{\text{int}} = \delta \mathcal{P}_{\text{ext}}. \quad (2.5)$$

With equations (2.3) and (2.4), the generalized virtual velocity is defined as the list $\delta v = \{ \delta \dot{\mathbf{u}}, \delta \dot{\gamma}_{\alpha} \}$, where $\delta \dot{\mathbf{u}}$ and $\delta \dot{\gamma}_{\alpha}$ denote the virtual counterparts of $\dot{\mathbf{u}}$ and $\dot{\gamma}_{\alpha}$, cf. [41], p. 594. The generalization of the principle of virtual power is given in Maugin [42] as theorem of energy, which states that the rate of kinetic energy results from the difference of power of external forces and power of internal forces. For the principle of virtual power, consequently, a vanishing rate of kinetic energy is assumed. Please note that the theorem of energy is not valid for bodies which contain singular surfaces. For a procedure consistent to Cermelli & Gurtin [40], however, the postulated principle of virtual power is used.

At first, a generalized virtual velocity without slip is considered, so that $\delta \dot{\gamma}_{\alpha} = 0$, cf. [40]. The application of the divergence theorem and using the balance of angular momentum, i.e. $\boldsymbol{\sigma} = \boldsymbol{\sigma}^T$, results in the principle of virtual power

$$- \int_{\mathcal{V}} (\rho \mathbf{b} + \text{div}(\boldsymbol{\sigma})) \cdot \delta \dot{\mathbf{u}} dv + \int_{\partial \mathcal{V}_t} (\boldsymbol{\sigma} \mathbf{n} - \bar{\mathbf{t}}) \delta \dot{\mathbf{u}} da = 0. \quad (2.6)$$

This equation has to be satisfied for all $\delta \dot{\mathbf{u}}$ and all subbodies. In a next step, a generalized virtual velocity with $\delta \dot{\mathbf{u}} = 0$ is considered. This results in

$$\begin{aligned} & \int_{\mathcal{V}} \sum_{\alpha=1}^N (\pi_{\alpha} - \text{div}(\boldsymbol{\xi}_{\alpha}) - \boldsymbol{\sigma} \cdot \mathbf{M}_{\alpha}^s) \delta \dot{\gamma}_{\alpha} dv \\ & + \int_{\partial \mathcal{V}_{\Pi}} \sum_{\alpha=1}^N (\boldsymbol{\xi}_{\alpha} \cdot \mathbf{n} - \bar{\Pi}_{\alpha}) \delta \dot{\gamma}_{\alpha} da - \int_S \sum_{\alpha=1}^N (\{\boldsymbol{\xi}_{\alpha} \delta \dot{\gamma}_{\alpha}\} \cdot \mathbf{n}_S - \{\Pi_{\alpha} \delta \dot{\gamma}_{\alpha}\}) da = 0, \end{aligned} \quad (2.7)$$

where \mathbf{n}_S denotes the normal vector of the grain boundary. Equation (2.7) has to be satisfied for all subbodies, i.e. for bulk material as well as for grain boundaries, separately. It follows

$$\int_{\mathcal{V}} \sum_{\alpha=1}^N (\pi_{\alpha} - \text{div}(\boldsymbol{\xi}_{\alpha}) - \boldsymbol{\sigma} \cdot \mathbf{M}_{\alpha}^s) \delta \dot{\gamma}_{\alpha} dv + \int_{\partial \mathcal{V}_{\Pi}} \sum_{\alpha=1}^N (\boldsymbol{\xi}_{\alpha} \cdot \mathbf{n} - \bar{\Pi}_{\alpha}) \delta \dot{\gamma}_{\alpha} da = 0, \quad (2.8)$$

and

$$\int_S \sum_{\alpha=1}^N (\boldsymbol{\xi}_{\alpha}^+ \cdot \mathbf{n}_S - \Pi_{\alpha}^+) \delta \dot{\gamma}_{\alpha}^+ da - \int_S \sum_{\alpha=1}^N (\boldsymbol{\xi}_{\alpha}^- \cdot \mathbf{n}_S - \Pi_{\alpha}^-) \delta \dot{\gamma}_{\alpha}^- da = 0, \quad (2.9)$$

for the bulk material and the grain boundaries, respectively. Since the virtual slip rates can be varied independently, cf. (Gurtin [41], ch. 105), equations (2.8) and (2.9) has to be satisfied for all $\delta \dot{\gamma}_{\alpha}$, $\alpha = 1, \dots, N$. With equations (2.6), (2.8) and (2.9) the following local field equations,

Neumann boundary conditions and grain boundary conditions are obtained

$$\pi_\alpha - \operatorname{div}(\xi_\alpha) - \tau_\alpha = 0, \quad \forall \alpha \in \{1, \dots, N\}, \quad \forall x \in \mathcal{V}, \quad (2.10)$$

$$\varrho \mathbf{b} + \operatorname{div}(\boldsymbol{\sigma}) = \mathbf{0}, \quad \forall x \in \mathcal{V}, \quad (2.11)$$

$$\xi_\alpha^\pm \cdot \mathbf{n}_S - \Pi_\alpha^\pm = 0, \quad \forall \alpha \in \{1, \dots, N\}, \quad \forall x \in \mathcal{S}, \quad (2.12)$$

$$\xi_\alpha \cdot \mathbf{n} - \bar{\Pi}_\alpha = 0, \quad \forall \alpha \in \{1, \dots, N\}, \quad \forall x \in \partial \mathcal{V}_\Pi, \quad (2.13)$$

$$\boldsymbol{\sigma} \mathbf{n} - \bar{\mathbf{t}} = \mathbf{0}, \quad \forall x \in \partial \mathcal{V}_t. \quad (2.14)$$

Here, for each slip system α , the resolved shear stress $\tau_\alpha := \boldsymbol{\sigma} \cdot \mathbf{M}_\alpha^s$ is introduced. On the Dirichlet boundary parts $\partial \mathcal{V}_u$ and $\partial \mathcal{V}_\gamma$, where \mathbf{u} and $\dot{\gamma}_\alpha$ are given, the virtual rates $\delta \dot{\mathbf{u}}$ and $\delta \dot{\gamma}_\alpha$ are assumed to vanish.

(c) Dissipation inequality

The dissipation inequality is derived based on the work of Gurtin [20], where a purely mechanical framework is considered. For isothermal processes, it is shown in Truesdell & Toupin [43], p. 639 that for any subregion of the body \mathcal{R} , the temporal increase in free energy is less than or equal to the power expended on it

$$\int_{\mathcal{R}} \varrho \dot{\psi} \, dv \leq \mathcal{P}_{\text{ext}}(\mathcal{R}), \quad (2.15)$$

where ψ denotes the free energy per unit volume and $\mathcal{P}_{\text{ext}}(\mathcal{R})$ denotes the power expended on the subregion. The localization of equation (2.15) to an arbitrary regular point within the bulk material results with equation (2.5) in

$$\boldsymbol{\sigma} \cdot \dot{\boldsymbol{\epsilon}}_e + \sum_{\alpha=1}^N (\pi_\alpha \dot{\gamma}_\alpha + \xi_\alpha \cdot \operatorname{grad}(\dot{\gamma}_\alpha)) - \varrho \dot{\psi}_V \geq 0, \quad (2.16)$$

where ψ_V denotes the free energy per unit volume of the bulk material. Additionally, with a shrinkage of \mathcal{R} to an arbitrary subsurface of the grain boundaries, equation (2.15) results in

$$\sum_{\alpha=1}^N \{\Pi_\alpha \dot{\gamma}_\alpha\} - \varrho_S \dot{\psi}_S \geq 0, \quad (2.17)$$

where ψ_S denotes the free energy per unit area of the grain boundaries.

(i) Bulk material

In the following, the free energy of the bulk material is assumed to depend on the elastic strain $\boldsymbol{\epsilon}_e$ and, for each slip system α , the internal hardening variable $\gamma_{\alpha c}$ and the slip gradient $\operatorname{grad}(\gamma_\alpha)$, i.e. $\psi_V = \psi_V(\boldsymbol{\epsilon}_e, \gamma_{\alpha c}, \operatorname{grad}(\gamma_\alpha))$. Inserting in equation (2.16) and using the local field equation of equation (2.10) results in the bulk material dissipation inequality

$$\begin{aligned} \mathcal{D} = & \left(\boldsymbol{\sigma} - \frac{\partial \varrho \psi_V}{\partial \boldsymbol{\epsilon}_e} \right) \cdot \dot{\boldsymbol{\epsilon}} + \sum_{\alpha=1}^N \left(\xi_\alpha - \frac{\partial \varrho \psi_V}{\partial \operatorname{grad}(\gamma_\alpha)} \right) \cdot \operatorname{grad}(\dot{\gamma}_\alpha) \\ & + \sum_{\alpha=1}^N \left(\frac{\partial \varrho \psi_V}{\partial \boldsymbol{\epsilon}_e} \cdot \mathbf{M}_\alpha^s + \operatorname{div}(\xi_\alpha) - \frac{\partial \varrho \psi_V}{\partial \gamma_{\alpha c}} \operatorname{sgn}(\dot{\gamma}_\alpha) \right) \dot{\gamma}_\alpha \geq 0, \quad (2.18) \\ & \forall \boldsymbol{\epsilon}, \dot{\boldsymbol{\epsilon}}, \gamma_\alpha, \dot{\gamma}_\alpha, \operatorname{grad}(\gamma_\alpha), \operatorname{grad}(\dot{\gamma}_\alpha). \end{aligned}$$

For simplicity, it is assumed that the Cauchy stress $\boldsymbol{\sigma}$ and the vector-valued microscopic stresses ξ_α are purely energetic stresses, cf. e.g. Bayerschen & Böhlke [44]. This results in the potential

relations

$$\boldsymbol{\sigma} = \frac{\partial \varrho \psi \gamma}{\partial \boldsymbol{\varepsilon}_e} \quad (2.19)$$

and

$$\boldsymbol{\xi}_\alpha = \frac{\partial \varrho \psi \gamma}{\partial \text{grad}(\gamma_\alpha)}, \quad \forall \alpha \in \{1, \dots, N\}. \quad (2.20)$$

Consequently, from equation (2.18), the reduced dissipation equation of the bulk material

$$\mathcal{D}_{\text{red}} = \sum_{\alpha=1}^N \left(\tau_\alpha + \text{div} \left(\frac{\partial \varrho \psi \gamma}{\partial \text{grad}(\gamma_\alpha)} \right) - \frac{\partial \varrho \psi \gamma}{\partial \gamma_{\alpha c}} \text{sgn}(\dot{\gamma}_\alpha) \right) \dot{\gamma}_\alpha \geq 0, \quad (2.21)$$

is obtained. For a modelling approach of polycrystals that includes dissipative microscopic stresses $\boldsymbol{\xi}_\alpha^{\text{dis}}$, cf., e.g. Bargmann & Reddy [45].

It is shown in Prahs & Böhlke [46] that the bulk material is dissipation free within a purely mechanical framework, i.e. $\mathcal{D}_{\text{red}} = 0$. This is equivalent to the assumption that the entire plastic work is stored inside the material. The assumptions of the purely mechanical theory in Prahs & Böhlke [46] are that the specific free energy can be additively decomposed into a mechanical and a thermal contribution, that the temperature is constant in space and time and that heat supplies are not present. With the assumption of a vanishing dissipation, a yield criterion function $\varphi_\alpha \leq 0$ is defined for each slip system in order to characterize plastic flow. For details on yield criterion functions the reader is referred to Simo & Hughes [47]. In this work, the rate-independent yield criterion of slip system α is specified by

$$\varphi_\alpha := \left| \tau_\alpha + \text{div} \left(\frac{\partial \varrho \psi \gamma}{\partial \text{grad}(\gamma_\alpha)} \right) \right| - \frac{\partial \varrho \psi \gamma}{\partial \gamma_{\alpha c}}. \quad (2.22)$$

The loading and unloading conditions can be formulated in Kuhn–Tucker form with

$$\varphi_\alpha \dot{\gamma}_{\alpha c} = 0, \quad \varphi_\alpha \leq 0, \quad \dot{\gamma}_{\alpha c} \geq 0, \quad \forall \alpha \in \{1, \dots, N\}. \quad (2.23)$$

(ii) Grain boundaries

Following the work of Gurtin [20], the free energy of the grain boundaries is assumed to depend on the grain boundary Burgers tensor \mathbf{G}_S in a quadratic form

$$\varrho_S \psi_S = \frac{1}{2} \kappa \| \mathbf{G}_S \|^2, \quad (2.24)$$

where the grain boundary strength κ is introduced as a material parameter. For the bulk material, \mathbf{G} measures the local Burgers vector, which represents the closure deficit of circuits deformed from a perfect lattice, per unit area in the microstructural configuration within a finite deformation setting. A gradient theory with a bulk material defect energy dependent on \mathbf{G} is presented in Gurtin [1], where $\mathbf{G} = \sum_\alpha \rho_\alpha^\ominus \mathbf{d}_\alpha \otimes \mathbf{d}_\alpha + \rho_\alpha^+ (\mathbf{n}_\alpha \times \mathbf{d}_\alpha) \otimes \mathbf{d}_\alpha$ is expressed in terms of pure screw dislocations ρ_α^\ominus and pure edge dislocations ρ_α^+ . Additionally, for a small deformation theory, $\mathbf{G} = \text{curl}(\mathbf{H}_p)$ is given. Based on this, Gurtin [20] defines the grain boundary Burgers tensor $\mathbf{G}_S = \{\mathbf{H}_p\}(\mathbf{n}_S \times)$, which reads in index notation $(\mathbf{G}_S)_{il} = \{\mathbf{H}_p\}_{ij} \epsilon_{jkl} (\mathbf{n}_S)_k$. A grain boundary is referred to as defect-free if $\mathbf{G}_S = \mathbf{0}$. The Burgers vector production within the grain boundary is given as $\|\dot{\mathbf{G}}_S\|$. With $\mathbf{H}_p = \sum_\alpha \gamma_\alpha \mathbf{d}_\alpha \otimes \mathbf{n}_\alpha$ and equation (2.24) it follows that the free energy of the grain boundaries depends on the right-hand limit and the left-hand limit of the plastic slips as well as on the orientation of slip systems and the orientation of the grain boundaries, i.e. $\psi_S = \psi_S(\gamma_\alpha^+, \gamma_\alpha^-, \mathbf{d}_\alpha^+, \mathbf{n}_\alpha^+, \mathbf{d}_\alpha^-, \mathbf{n}_\alpha^-, \mathbf{n}_S)$. With equation (2.17), the dissipation of the grain boundaries

reads

$$\mathcal{D}_S = \sum_{\alpha=1}^N \left(\{ \Pi_{\alpha} \dot{\gamma}_{\alpha} \} - \frac{\partial \varrho_S \psi_S}{\partial \gamma_{\alpha}^+} \dot{\gamma}_{\alpha}^+ - \frac{\partial \varrho_S \psi_S}{\partial \gamma_{\alpha}^-} \dot{\gamma}_{\alpha}^- \right) \geq 0. \quad (2.25)$$

With equation (2.12) this results in

$$\mathcal{D}_S = \sum_{\alpha=1}^N \left(-\xi_{\alpha}^+ \cdot \mathbf{n}_S^+ - \frac{\partial \varrho_S \psi_S}{\partial \gamma_{\alpha}^+} \right) \dot{\gamma}_{\alpha}^+ + \sum_{\beta=1}^N \left(-\xi_{\beta}^- \cdot \mathbf{n}_S^- - \frac{\partial \varrho_S \psi_S}{\partial \gamma_{\beta}^-} \right) \dot{\gamma}_{\beta}^- \geq 0, \quad (2.26)$$

where $\mathbf{n}_S = \mathbf{n}_S^- = -\mathbf{n}_S^+$ holds true, cf. e.g. [48]. In the following, based on the work of Prah & Böhlke [46], dissipation free grain boundaries are considered for the purely mechanical framework which means again that the inelastic work is stored as defect energy in the grain boundaries. Consequently, the presented framework considers only energetic dislocation grain-boundary interactions, while neglecting the dissipative mechanisms, e.g. dislocation absorption within grain boundaries. An approach to the modelling of dislocation absorption that could be integrated into the presented framework is developed in Peng *et al.* [49]. The coupling of two mechanisms, slip transmission and dislocation absorption, respectively, is presented in Peng *et al.* [22]. Two approaches are presented in order to solve equation (2.26) for the unknown $2N$ grain boundary slip values arising from a discontinuous slip distribution across grain boundaries.

Approach I (independent plastic slips): A conventional approach developed by Gurtin [20], here called approach I, is the assumption of independent slip rates at the grain boundaries. For each slip system on both sides of the grain boundary, i.e. for a total of $2N$ slip systems, a yield function is formulated such that equation (2.26) is satisfied. With the assumption of dissipation free grain boundaries and equation (2.12) the loading conditions of the grain boundaries can be formulated in Kuhn–Tucker form

$$\begin{aligned} \varphi_{S\alpha}^+ \dot{\gamma}_{\alpha}^+ &= 0, & \varphi_{S\alpha}^+ &\leq 0, & \dot{\gamma}_{\alpha}^+ &\geq 0, & \forall \alpha \in \{1, \dots, N\}, \\ \varphi_{S\beta}^- \dot{\gamma}_{\beta}^- &= 0, & \varphi_{S\beta}^- &\leq 0, & \dot{\gamma}_{\beta}^- &\geq 0, & \forall \beta \in \{1, \dots, N\}, \end{aligned} \quad (2.27)$$

with the yield functions

$$\varphi_{S\alpha}^+ := \xi_{\alpha}^+ \cdot \mathbf{n}_S^+ + \varrho_S \frac{\partial \psi_S}{\partial \gamma_{\alpha}^+} \quad (2.28)$$

and

$$\varphi_{S\beta}^- := \xi_{\beta}^- \cdot \mathbf{n}_S^- + \varrho_S \frac{\partial \psi_S}{\partial \gamma_{\beta}^-}. \quad (2.29)$$

This approach is used, e.g. in the numerical simulations of Özdemir & Yalçinkaya [50] for the two-dimensional case, or Gottschalk *et al.* [51] and McBride *et al.* [52] in three dimensions.

As later shown, the assumption of independent plastic slips at grain boundaries results in artefacts of slip distributions across grain boundaries for the limit case of two adjacent grains that hold no misorientation. For this limit case of vanishing misorientation, and under the assumption of identical material properties, the adjacent grains should behave as if they were one grain, i.e. displacement, slips and stresses should be continuous across the non-existing boundary with zero interface energy. With $\psi_S = 0$, equations (2.28) and (2.29) directly results in $\xi_{\alpha}^+ \cdot \mathbf{n}_S^+ = 0$, $\forall \alpha \in \{1, \dots, N\}$ and $\xi_{\beta}^- \cdot \mathbf{n}_S^- = 0$, $\forall \beta \in \{1, \dots, N\}$. With equation (2.20) and the common approach of a quadratic dependency of the bulk material energy on the gradients of plastic slips, cf. e.g. [53], this results in $\text{grad}(\gamma_{\alpha}^+) \cdot \mathbf{n}_S^+ = 0$ and $\text{grad}(\gamma_{\beta}^-) \cdot \mathbf{n}_S^- = 0$. While this result may be valid for symmetric grain structures, it leads to artefacts of slip distributions for more general structures, as later shown. In order to overcome this modelling shortcoming, a new grain boundary modelling approach of coupled slip systems at grain boundaries is introduced.

Approach II (coupled slips): Without the assumption of independent plastic slip rates at the grain boundaries, equation (2.26) reads for the special case of dissipation free grain boundaries

$$\sum_{\alpha=1}^N \left(\xi_{\alpha}^+ \cdot \mathbf{n}_S^+ + \varrho_S \frac{\partial \psi_S}{\partial \gamma_{\alpha}^+} \right) \dot{\gamma}_{\alpha}^+ + \sum_{\beta=1}^N \left(\xi_{\beta}^- \cdot \mathbf{n}_S^- + \varrho_S \frac{\partial \psi_S}{\partial \gamma_{\beta}^-} \right) \dot{\gamma}_{\beta}^- = 0. \quad (2.30)$$

In this dissipation free case, the dissipation equation is called pseudo dissipation equation or non-dissipation condition. In contrary to approach I, additional equations which describe the compatibility of adjacent slip systems are required. In order to derive the constitutive equations for slip system coupling again the limit case of two adjacent grains with identical material properties that hold no misorientation is considered. For this limit case, each slip system α has a neighbouring slip system with which the distribution of slips should be continuous. For the limit case, the numbering of slip systems is chosen such that $\gamma_{\alpha}^{+} = \gamma_{\alpha}^{-}$, $\forall \alpha = 1 \dots N$. With $\psi_S = 0$ for the limit case of vanishing misorientation, equation (2.30) results in

$$\sum_{\alpha=1}^N (\xi_{\alpha}^{+} - \xi_{\alpha}^{-}) \cdot \mathbf{n}_S = 0. \quad (2.31)$$

In order to fulfil this limit case, while accounting for a compatibility based on the amount of misorientation between adjacent slip systems, a geometric measure of slip system compatibility $\lambda_{\alpha\beta}$ is introduced for a slip system pair $\{\alpha, \beta\}$. The dependency of $\lambda_{\alpha\beta}$ based on the amount of misorientation is introduced based on the work of Werner & Prantl [23] as

$$\lambda_{\alpha\beta} = \cos\left(\frac{\pi}{2\delta_c} \arccos(I_{\alpha}^{+} \cdot I_{\beta}^{-})\right) \cos\left(\frac{\pi}{2\kappa_c} \arccos(d_{\alpha}^{+} \cdot d_{\beta}^{-})\right), \quad (2.32)$$

where δ_c and κ_c are the critical angles above which no dislocation transmission occurs and $I_{\alpha}^{\pm} = (\mathbf{n}_{\alpha}^{\pm} \times \mathbf{n}_S) / \|\mathbf{n}_{\alpha}^{\pm} \times \mathbf{n}_S\|$ denotes the intersection lines that each plane makes with the interface. The compatibility $\lambda_{\alpha\beta}$ varies in between the limits $\lambda_{\alpha\beta} = 0$ for microhard slip system coupling and $\lambda_{\alpha\beta} = 1$ for microfree slip system coupling. Whereas in Werner & Prantl [23], an overall slip transmission coefficient is constructed based on all combinations of slip systems, in this work geometrically efficient pathways for slip transmission across grain boundaries are constructed. For each slip system α on the right-hand side of the grain boundary, the adjacent slip system β on the left-hand side of the grain boundary with highest compatibility is searched, i.e. $\max_{\beta}(\lambda_{\alpha\beta})$. Consequently, the pairing of slip systems $\{\alpha, \beta\}$ results in a minimum hindrance for slip transmission. Please note that, for simplicity, it is assumed that no transmission of slip from one incoming slip system into multiple slip systems occurs and that the number of slip systems on each side of the grain boundary is identical. Equation (2.31) motivates the constitutive equations for slip system coupling across grain boundaries for each slip system pair $\{\alpha, \beta\}$

$$(\xi_{\alpha}^{+} - \xi_{\beta}^{-}) \cdot \mathbf{n}_S - \xi_0 \frac{1 - \lambda_{\alpha\beta}}{\lambda_{\alpha\beta}} = 0, \quad \forall \alpha \in \{1, \dots, N\}, \max_{\beta}(\lambda_{\alpha\beta}), \quad (2.33)$$

where ξ_0 is introduced as the grain boundary misorientation parameter. Equation (2.33) accounts for two aspects, which according to Beyerlein *et al.* [54] are important for slip transmission. First the geometric aspect that the slip systems α and β have to be well aligned, quantified by $\lambda_{\alpha\beta}$. Second the activation barrier for slip transmission, quantified by the grain boundary misorientation parameter ξ_0 . The ability of an interface to transmit dislocations may change with strain [54]. A grain boundary hardening could be introduced by a dependence of ξ_0 on the mean value of slip at the boundary, cf. e.g. Bayerschen *et al.* [55]. In this work, however, ξ_0 is chosen as a constant material parameter, resulting in a constant activation barrier. Equation (2.33) gives N equations for the coupling of slip systems at grain boundaries, consequently, equation (2.30) has to be formulated in such a way as to obtain one additional equation for each of the N slip system pairs $\{\alpha, \beta\}$. The sorting of equation (2.33) to account for the slip systems pairs $\{\alpha, \beta\}$ with $\max_{\beta}(\lambda_{\alpha\beta})$ results in

$$\sum_{\alpha=1}^N \left(\left(\xi_{\alpha}^{+} \cdot \mathbf{n}_S^{+} + \varrho_S \frac{\partial \psi_S}{\partial \gamma_{\alpha}^{+}} \right) \dot{\gamma}_{\alpha}^{+} + \left(\xi_{\beta}^{-} \cdot \mathbf{n}_S^{-} + \varrho_S \frac{\partial \psi_S}{\partial \gamma_{\beta}^{-}} \right) \dot{\gamma}_{\beta}^{-} \right) = 0, \quad \max_{\beta}(\lambda_{\alpha\beta}). \quad (2.34)$$

It is assumed that each summand is zero, i.e.

$$\left(\xi_{\alpha}^{+} \cdot \mathbf{n}_S^{+} + \varrho_S \frac{\partial \psi_S}{\partial \gamma_{\alpha}^{+}} \right) \dot{\gamma}_{\alpha}^{+} + \left(\xi_{\beta}^{-} \cdot \mathbf{n}_S^{-} + \varrho_S \frac{\partial \psi_S}{\partial \gamma_{\beta}^{-}} \right) \dot{\gamma}_{\beta}^{-} = 0, \quad \forall \alpha \in \{1, \dots, N\}, \max_{\beta}(\lambda_{\alpha\beta}). \quad (2.35)$$

Consequently, in combination with equation (2.33), a system of equations is obtained which can be solved for the unknown $2N$ grain boundary slip values. The proposed grain boundary modelling approach with coupled plastic slip rates at the grain boundaries does not result in the artefacts which can be observed in approach I. For the limit case of vanishing misorientation, i.e. $\lambda_{\alpha\beta} = 1 \forall \alpha \in \{1, \dots, N\}$, $\max_{\beta}(\lambda_{\alpha\beta})$ and $\psi_S = 0$ it directly follows from equations (2.33) and (2.35) that the slips γ_{α} and microscopic stresses ξ_{α} are continuous across the non-existing boundary. In order to compare the grain boundary model approaches for various slip system configurations an analytical solution of a laminate microstructure is constructed.

To summarize: in a first step, based on the maximization of a measure of slip system compatibility, a total of N slip system pairs are constructed for the $2N$ slip systems at a grain boundary. For each of these pairs of slip systems, a constitutive coupling equation is introduced by the set of equations given by equation (2.33). In a second step, the scalar pseudo grain boundary dissipation equation, given in equation (2.30), is split into N partial dissipation equations, one for each slip system pair, cf. equation (2.35). Note that the partitioning of the pseudo dissipation equation results in equations that are sufficient to ensure the non-dissipation condition. Consequently, N coupling equations and N partial grain boundary dissipation equations are given, which is sufficient to solve equation (2.30) for the unknown $2N$ grain boundary slip values.

The presented slip system coupling approach requires an equal number of slip systems on both sides of the grain boundaries. Throughout the manuscript, following the work Gurtin [20], it has been assumed that the number of slip systems is constant within the material. However, it would be possible to introduce individual groups of interacting slip systems instead of unique pairs. The equations for slip system coupling and pseudo grain boundary dissipation would have to be reformulated accordingly.

3. Comparison of grain boundary models with an analytical solution

(a) Simulation set-up and constitutive assumptions

The gradient crystal plasticity framework is applied to an elasto-plastic laminate microstructure in order to discuss the differences between the two grain boundary flow rules. The analytical solution of the periodic laminate structure is given in appendix A. For the sake of simplicity, the exact solution of the model problem is discussed under the assumption of single-slip with slip γ and monotonic loading.

As shown in the schematic illustration of figure 1 the laminate, which is exposed to plane strain, consists of three periodic layers. Two elasto-plastic layers A and B, coloured in light grey, are separated by a grain boundary \mathcal{S} with plane normal \mathbf{n}_S . The elastic layer E, coloured in dark grey, results in microhard boundary conditions. The origin of the global coordinate system $\{e_1, e_2\}$ is located at the grain boundary of the adjacent elasto-plastic grains A and B. The widths of the layers A, B and E are denoted by h_A, h_B and h_E , respectively. Each elasto-plastic grain contains a single slip system, characterized by slip direction vectors \mathbf{d}_A and \mathbf{d}_B and slip plane normal vectors \mathbf{n}_A and \mathbf{n}_B . The misorientation between the slip system $\{\mathbf{d}_A, \mathbf{n}_A\}$ and $\{\mathbf{d}_B, \mathbf{n}_B\}$ is varied by the angle ϑ_A . In Duda & Šilhavý [56], a kinematic analysis of dislocation walls between regions with only one active slip system in each is performed. It is shown that the existence of a dislocation wall requires one of three cases for the slip system configuration. The slip system configuration used in this work satisfies Case B, i.e. $\mathbf{n}_A \cdot \mathbf{d}_A = \mathbf{n}_B \cdot \mathbf{d}_B = 0$, therefore a dislocation wall in between grains A and B can exist.

The free energy in the bulk material within the small deformation framework is assumed to be additively decomposed into three terms

$$\psi_V(\boldsymbol{\varepsilon}_e, \gamma, \text{grad}(\gamma)) = \psi_e(\boldsymbol{\varepsilon}_e) + \psi_g(\text{grad}(\gamma)) + \psi_R(\gamma), \quad (3.1)$$

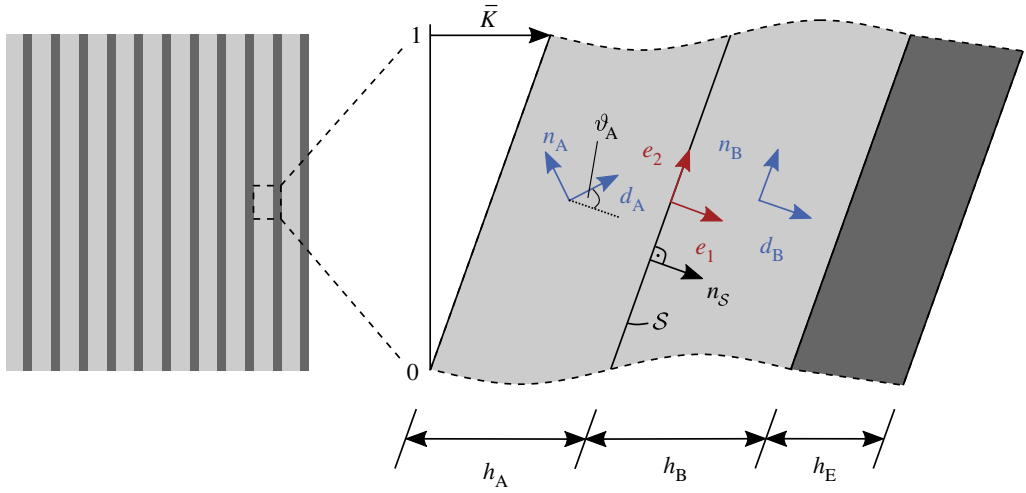


Figure 1. Undeformed periodic laminate material and deformed unit cell. The misorientation between the slip system $\{d_A, n_A\}$ and $\{d_B, n_B\}$ is described by the angle ϑ_A .

i.e. an elastic energy contribution ψ_e , a defect energy contribution ψ_g and an isotropic hardening energy contribution ψ_h . The elastic energy contribution is given by

$$\varrho \psi_e = \frac{1}{2} \boldsymbol{\varepsilon}_e \cdot \mathbb{C}[\boldsymbol{\varepsilon}_e] = \frac{1}{2} (\boldsymbol{\varepsilon} - \boldsymbol{\varepsilon}_p) \cdot \mathbb{C}[\boldsymbol{\varepsilon} - \boldsymbol{\varepsilon}_p]. \quad (3.2)$$

For the sake of simplicity, elastic isotropic material behaviour is considered. Consequently, the stiffness matrix reads $\mathbb{C} = \lambda \mathbf{I} \otimes \mathbf{I} + 2\mu \mathbb{I}^S$, where λ and μ are so-called Lamé parameters. Hooke's Law for linear elastic isotropic solid bodies reads $\boldsymbol{\sigma} = \lambda \text{tr}(\boldsymbol{\varepsilon}_e) \mathbf{I} + 2\mu \boldsymbol{\varepsilon}_e$. For the defect energy density the phenomenological, quadratic approach

$$\varrho \psi_g = \frac{1}{2} K_g \|\text{grad}(\gamma)\|^2, \quad (3.3)$$

is chosen, where K_g is a constant material parameter. Isotropic hardening is characterized by the isotropic hardening energy

$$\varrho \psi_h = \frac{1}{2} K_0 \gamma^2 + \tau_0 \gamma, \quad (3.4)$$

where K_0 and τ_0 are introduced as material parameters.

Additionally to the free energy of the bulk material, an extrinsic grain boundary dislocation energy is introduced according to equation (2.24). For the special case of single slip the magnitude of the grain boundary Burgers tensor reads

$$\|\mathbf{G}_S\|^2 = C_{AA} \gamma_{SA}^2 + C_{BB} \gamma_{SB}^2 - 2C_{AB} \gamma_{SA} \gamma_{SB}, \quad (3.5)$$

cf. [20], with right-hand limit of plastic slip $\gamma^+ = \gamma_{SB}$ and left-hand limit of plastic slip $\gamma^- = \gamma_{SA}$. The slip-interaction moduli depend on the orientation of the slip systems within the two grains and the grain boundary normal vector \mathbf{n}_S

$$C_{AA} = (\mathbf{n}_A \times \mathbf{n}_S) \cdot (\mathbf{n}_A \times \mathbf{n}_S), \quad (3.6)$$

$$C_{BB} = (\mathbf{n}_B \times \mathbf{n}_S) \cdot (\mathbf{n}_B \times \mathbf{n}_S) \quad (3.7)$$

and

$$C_{AB} = (\mathbf{d}_A \cdot \mathbf{d}_B) (\mathbf{n}_A \times \mathbf{n}_S) \cdot (\mathbf{n}_B \times \mathbf{n}_S). \quad (3.8)$$

C_{AA} and C_{BB} account for interactions between slip systems within the respective grain, whereas C_{AB} accounts for the interactions of slip systems between the two grains.

The material parameters of the aluminium-type bulk material are chosen according to Bayerschen *et al.* [55]. Isotropic elastic material behaviour is homogeneous within the laminate material with $\mu = 27$ GPa. The plastic behaviour in both elasto-plastic layers is also chosen to be homogeneous with $\tau_0 = 10$ MPa, $K_0 = 1075$ MPa and $K_g = 84 \mu\text{N}$. The grain boundary strength is chosen according to Özdemir & Yalçinkaya [50] as $\kappa = 2100 \text{ N m}^{-1}$. The remaining material parameters of grain boundary model approach II are chosen according to Alipour *et al.* [25] and Beyerlein *et al.* [54] as $\delta_c = 15^\circ$, $\kappa_c = 45^\circ$ and $\xi_0 = 10 \text{ N m}^{-1}$.

(b) Comparison of grain boundary modelling approaches

(i) Limit case of coinciding slip systems

At first the limit case of coinciding slip systems is investigated. For this study, the width of the elasto-plastic grain A is chosen to be $h_A = 0.5 \mu\text{m}$, while the width of the elasto-plastic grain B is varied between $h_B = h_A$ and $h_B = h_A/8$. The width of the elastic layer is set to $h_E = 0.5 \mu\text{m}$, however, with the plastic slip being zero, the elastic layer is not depicted in the solutions.

For a macroscopic shear of $\bar{K} = 0.005$, figure 2a shows the exact solution of the plastic slip distribution $\gamma(x_1)$ over the laminate for the grain boundary model approach I. The grain boundary, which should not be observable for the limit case of coinciding slip systems, is located at $x_1 = 0 \mu\text{m}$. For the limit case of vanishing misorientation, the grain boundary model approach I, given in equations (2.28) and (2.29), reads

$$\xi_B \cdot \mathbf{n}_S + \kappa(\gamma_{SA} - \gamma_{SB}) = 0 \quad (3.9)$$

and

$$\xi_A \cdot \mathbf{n}_S + \kappa(\gamma_{SA} - \gamma_{SB}) = 0. \quad (3.10)$$

A solution is obtained for $\xi_A \cdot \mathbf{n}_S = \xi_B \cdot \mathbf{n}_S$, i.e. the slip gradients in normal direction have to coincide at the grain boundary. This can be observed in figure 2a for all $h_B \leq h_A$. In the case of a symmetric grain structure, i.e. $h_A = h_B$, the distribution of the plastic slip is continuous across the grain boundary, with $\xi_A \cdot \mathbf{n}_S = \xi_B \cdot \mathbf{n}_S = 0$. For $h_B < h_A$, however, the plastic slip is discontinuous with $\gamma_{SA} > \gamma_{SB}$. It can be seen that with decreasing grain width h_B , the discontinuity of the plastic slip at the grain boundary increases. The single-crystal consistency check is failed.

Figure 2b shows the exact solutions of the plastic slip distribution $\gamma(x_1)$ over the laminate using grain boundary model approach II. In contrast to approach I, the distribution of the plastic slip in solution II not only is continuous across the grain boundary for the case of $h_A = h_B$, but also for all $h_B \leq h_A$. Approach II for the grain boundary model, given in equations (2.33) and (2.35), reads for the limit case of vanishing misorientation

$$\xi_B \cdot \mathbf{n}_S - \xi_A \cdot \mathbf{n}_S = 0, \quad (3.11)$$

$$-(\xi_B \cdot \mathbf{n}_S + \kappa(\gamma_{SA} - \gamma_{SB}))\dot{\gamma}_{SB} + (\xi_A \cdot \mathbf{n}_S + \kappa(\gamma_{SA} - \gamma_{SB}))\dot{\gamma}_{SA} = 0. \quad (3.12)$$

Equation (3.11) relates the discontinuity of the slip gradient at the grain boundary to the geometric measure of slip system compatibility, which is zero for the limit case of vanishing misorientation. As a result the slip gradients in normal direction of both sides of the grain boundary coincide and equation (3.12) results in

$$(\xi_A \cdot \mathbf{n}_S + \kappa(\gamma_{SA} - \gamma_{SB}))(\dot{\gamma}_{SA} - \dot{\gamma}_{SB}) = 0. \quad (3.13)$$

Consequently, for the limit case of coinciding slip systems, a possible solution obtained with the grain boundary model approach II is a continuous and continuous differentiable distribution of the plastic slip across the grain boundary. The single-crystal consistency check is passed.

(ii) Variation of slip system misorientation

Additionally to the limit case of coinciding slip systems, the influence of a varying grain misorientation with misorientation angles $\vartheta_A = \{0^\circ, 10^\circ, 20^\circ, 30^\circ\}$ is investigated. For simplicity,

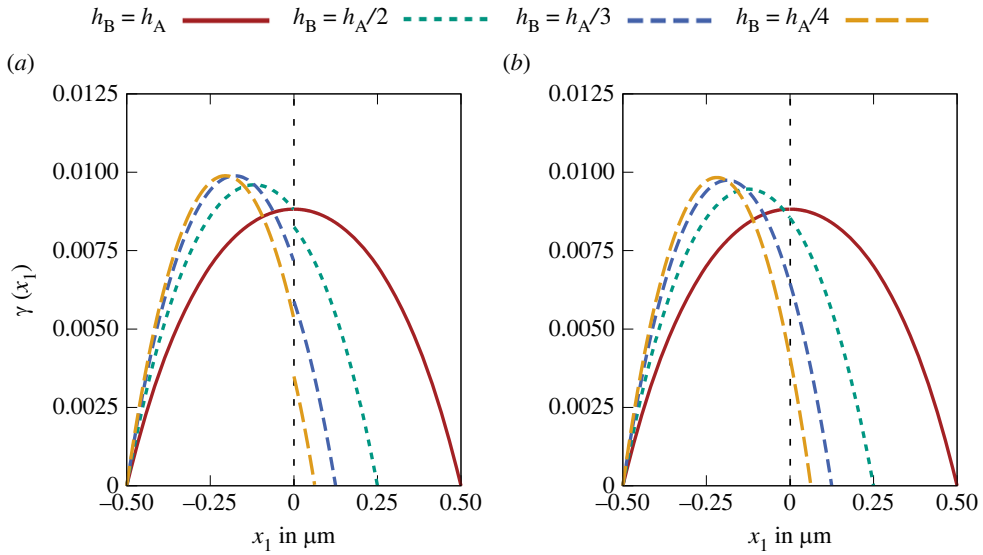


Figure 2. Comparison of grain boundary model approach I (a) and approach II (b) for the limit case of coinciding slip systems with a macroscopic shear of $\bar{K} = 0.005$. The exact solutions for the plastic slip $\gamma(x_1)$ are shown for a varying grain width h_B .

the three layers of the laminate are equally sized with $h_A = h_B = h_E = 0.5 \mu\text{m}$. The laminate is exposed to a macroscopic shear strain of $\bar{K} = 0.005$.

Figure 3 shows the exact solutions of the plastic slip distributions over the laminate structure with the use of grain boundary model approach I and grain boundary model approach II, respectively. For $\vartheta_A = 0^\circ$, i.e. limit case of coinciding slip systems at the grain boundary, the single-crystal solution is obtained. For approach I, depicted in figure 3a, all solutions which include a misorientation between adjacent slip systems result in a discontinuous distribution of the plastic slip at the grain boundary. It can be seen that with increasing grain misorientation angle, the discontinuity of the plastic slip at the grain boundary slightly increases. For approach II, shown in figure 3b, however, a more distinct discontinuity is observed at the grain boundary. Whereas for approach I, the discontinuity of slip is almost constant for a varying misorientation angle, for approach II, the discontinuity of slip increases strongly with lower slip system compatibility. Additionally, based on the amount of the misorientation, the gradient of plastic slip increases. This can be related to the amount of dislocations, which are piled-up at the grain boundary.

In order to investigate the differences of the solutions obtained by grain boundary model approach I and approach II, the laminate is exposed to an increasing macroscopic shear strain of $\bar{K} \in \{0, \dots, 0.005\}$. This allows the investigation of the grain boundary states during loading. In figure 4, the effective stress–strain curves are shown with the use of grain boundary model approach I and grain boundary model approach II, respectively. While for approach I, shown in figure 4a, only two sectors of the stress–strain curve are observable, three grain boundary states can be identified for approach II, which is shown in figure 4b:

- Elastic: No yield condition is satisfied. The plastic slip is zero.
- Microhard: The yield condition is satisfied only in the bulk material but not in the grain boundary. Dislocations pile-up at the grain boundary.
- Microcontrolled: The yield condition is satisfied in the bulk material as well as in the grain boundary. Grain boundary plasticity occurs.

The resistance of the grain boundary against dislocation transmission strongly depends on the geometric measure of slip system compatibility. This results in an orientation-dependent

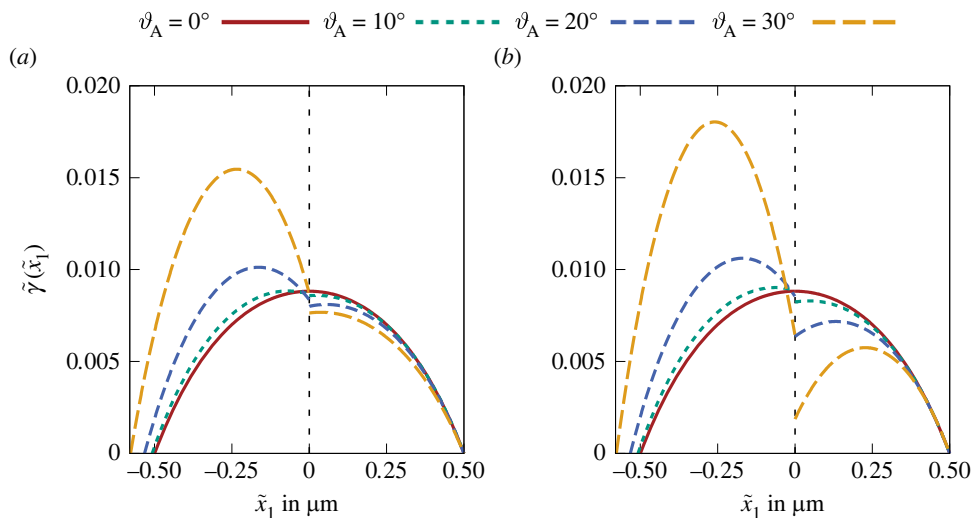


Figure 3. Comparison of grain boundary model approach I (a) and approach II (b) for a varying misorientation angle ϑ_A with a macroscopic shear of $\bar{K} = 0.005$. The exact solutions for the plastic slip $\tilde{\gamma}(\tilde{x}_1)$ are shown in the local coordinate systems.

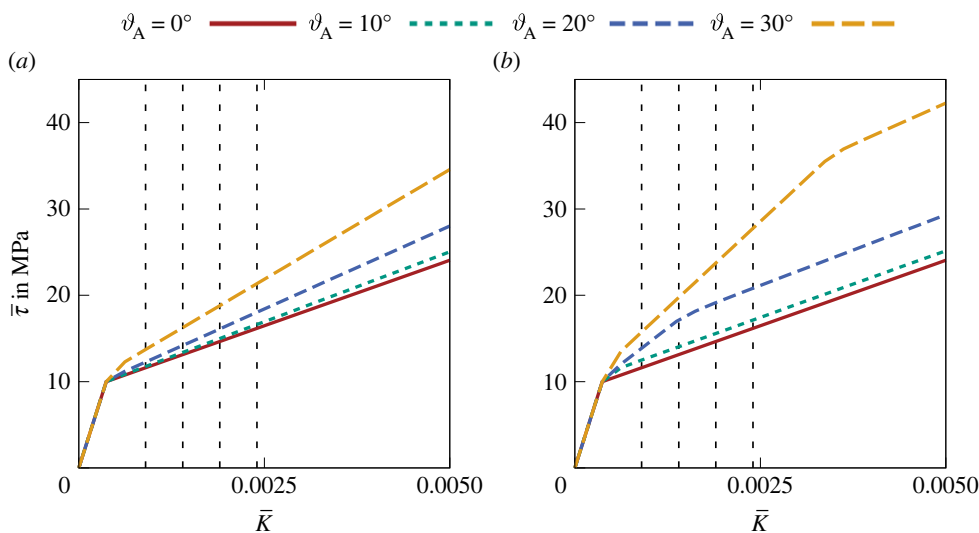


Figure 4. Comparison of effective stress obtained with grain boundary model approach I (a) and approach II (b) for misaligned grains with a varying misorientation angle ϑ_A .

transition point of the microcontrolled grain boundary state. For $\vartheta_A = 0^\circ$, i.e. limit case of coinciding slip systems, dislocations can cross the grain boundary without hindrance. The amount of dislocations piled-up at the grain boundary before the critical stress for grain boundary transmission is reached is higher for lower slip system compatibility, i.e. a higher misorientation angle. For $\vartheta_A = 10^\circ$, the effective stress which results from the different grain boundary model approaches is similar, the transition from a microhard to a microcontrolled grain boundary state occurs immediately. For $\vartheta_A = 20^\circ$ and $\vartheta_A = 30^\circ$, however, a distinct microhard grain boundary state is observable in the solution obtained by grain boundary model approach II. The coupling of the slip system results in higher effective stresses for slip system configurations with low slip system compatibility.

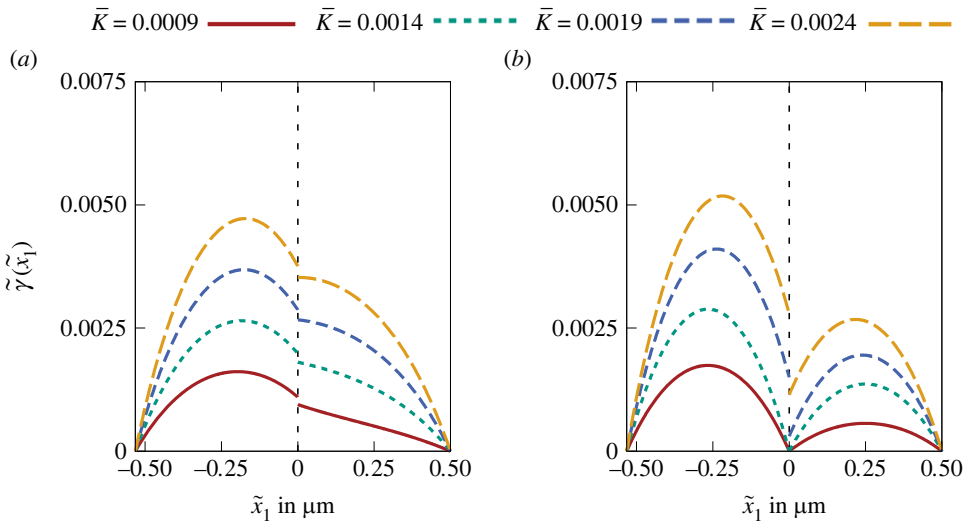


Figure 5. Exact solutions for the evolution of the plastic slip $\tilde{\gamma}(\tilde{x}_1)$ in the local coordinate systems for grain boundary model approach I (a) and approach II (b) with grain misorientation $\vartheta_A = 20^\circ$.

To illustrate the different grain boundary states that occur during the loading process, the distribution of the plastic slip over the laminate structure is shown for $\vartheta_A = 20^\circ$ in figure 5 for the four loading states labelled in figure 4. For approach I shown in figure 5a, plastic slip evolves at the grain boundary as soon as the initial critical resolved shear stress occurs. The grain boundary always behaves microfree. For approach II, shown in figure 5b, the grain boundary at first is microhard. After a sufficient amount of dislocations piled-up at the grain boundary, the grain boundary flow condition is fulfilled and grain boundary slip is permitted. For this microcontrolled grain boundary state, the discontinuity of the plastic slip evolves. The two stages of grain boundary behaviour which are observed in Sun *et al.* [26], i.e. build-up of dislocations near the grain boundary and a vanishing peak at higher strain levels, can be modelled.

4. Summary and conclusion

A gradient crystal plasticity framework was applied to a three-phase periodic laminate microstructure in order to investigate dislocation transmission through grain boundaries with an analytical solution. An extrinsic grain boundary dislocation energy according to Gurtin [20] based on the geometric dislocation tensor was used in order to account for a grain boundary resistance against dislocation transmission based on the misorientation angle of adjacent slip systems.

It was shown that with the conventional grain boundary modelling approach based on the assumption of independent plastic slips at the grain boundary the single-crystal consistency check for the limit case of two adjacent grains that hold no misorientation is failed. A continuous distribution of the plastic slip across the non-existing grain boundary is expected, however, a discontinuous distribution is observed. In order to overcome this modelling shortcoming, a new grain boundary modelling approach including a coupling of slip systems was introduced. Hereby, the discontinuity of the plastic slip gradient at the grain boundary is correlated to a geometric measure of slip system compatibility. The presented grain boundary modelling approach is able to predict the two limit cases of a microfree grain boundary behaviour for equally orientated grains and a microhard grain boundary behaviour for strongly misaligned grains.

Various misorientation angles between adjacent slip systems were investigated in order to evaluate the influence of the slip system compatibility on the mechanical response of the crystalline structure. Under the assumption of independent slip rates at the grain boundary

the boundary always behaves microfree. With the introduction of slip system coupling at first a microhard grain boundary state was observed. This results in a pile-up of dislocations at the grain boundary until a critical state is reached. The critical pile-up stress for dislocation transmission depends on the misorientation angle between the slip systems of adjacent grains. Consequently, the introduction of slip system coupling allows the modelling of dislocation transition across grain boundaries based on the compatibility of adjacent slip systems. The presented grain boundary modelling approach provides a promising framework for the modelling of polycrystalline materials within a finite-element implementation, where various misorientation angles and grain sizes are involved.

Data accessibility. MATLAB scripts for the analytical solution of the single-slip gradient crystal plasticity framework, figure data and corresponding Gnuplot scripts, labelled according to figure number in the manuscript are provided in the electronic supplementary material [57].

Authors' contributions. H.E.: conceptualization, data curation, formal analysis, investigation, methodology, software, validation, visualization, writing—original draft; T.B.: conceptualization, funding acquisition, methodology, project administration, resources, supervision, writing—review and editing.

All authors gave final approval for publication and agreed to be held accountable for the work performed therein.

Conflict of interest declaration. We declare we have no competing interests.

Funding. Funded by the Deutsche Forschungsgemeinschaft (DFG, German Research Foundation) - Project-ID 374768210 (BO 1466/14-2), within the Priority Programme SPP 2013 'Targeted Use of Forming Induced Residual Stresses in Metal Components'.

Appendix A. Analytical solution of the periodic laminate structure

(a) Displacement field, strain and stress

In order to account for a misorientation between the two adjacent elasto-plastic grains, a local coordinate system $\{\tilde{e}_1, \tilde{e}_2\}$ is introduced within each grain. The transformation from the global into the local coordinate system is performed by a rotation about the e_3 -axis by the angles ϑ_A and ϑ_B for grains A and B, respectively. For simple shear, the displacement field is assumed in the form

$$\tilde{u} = \tilde{u}_1(\tilde{x}_2)\tilde{e}_1 + \tilde{u}_2(\tilde{x}_1)\tilde{e}_2. \quad (\text{A } 1)$$

An elastic isotropic and homogeneous material is assumed. The infinitesimal strain tensor in the local coordinate system is defined by

$$\tilde{\epsilon} = \text{sym}(\text{grad}(\tilde{u})) = \frac{1}{2} \left(\frac{d\tilde{u}_1}{d\tilde{x}_2} + \frac{d\tilde{u}_2}{d\tilde{x}_1} \right) (\tilde{e}_1 \otimes \tilde{e}_2 + \tilde{e}_2 \otimes \tilde{e}_1). \quad (\text{A } 2)$$

With the assumption of a monotonous evolution of the plastic slip, the plastic strain tensor results from equation (2.1) as

$$\tilde{\epsilon}_p = \tilde{\gamma} \tilde{M}^s = \frac{1}{2} \tilde{\gamma} (\tilde{e}_1 \otimes \tilde{e}_2 + \tilde{e}_2 \otimes \tilde{e}_1). \quad (\text{A } 3)$$

With the local Cauchy stress tensor

$$\tilde{\sigma} = \tilde{\mathbb{C}}[\tilde{\epsilon} - \tilde{\epsilon}_p] = \mu \left(\frac{d\tilde{u}_1}{d\tilde{x}_2} + \frac{d\tilde{u}_2}{d\tilde{x}_1} - \tilde{\gamma} \right) (\tilde{e}_1 \otimes \tilde{e}_2 + \tilde{e}_2 \otimes \tilde{e}_1), \quad (\text{A } 4)$$

the resolved shear stress results in

$$\tilde{\tau} = \tilde{\sigma} \cdot \tilde{M}^s = \mu \left(\frac{d\tilde{u}_1}{d\tilde{x}_2} + \frac{d\tilde{u}_2}{d\tilde{x}_1} - \tilde{\gamma} \right). \quad (\text{A } 5)$$

(b) Analytical solution for plastic slip

With the introduced free energy of the bulk material, cf. equations (3.2)–(3.4), and the potential relation, given in equation (2.20), it follows:

$$\frac{\partial \varrho \psi_V}{\partial \gamma} = K_0 \gamma + \tau_0, \quad \xi = \frac{\partial \varrho \psi_V}{\partial \text{grad}(\gamma)} = K_g \text{grad}(\gamma). \quad (\text{A } 6)$$

With equation (2.22), the inhomogeneous second-order linear ordinary differential equation in the local coordinate system is obtained

$$K_g \frac{d^2 \tilde{\gamma}}{d\tilde{x}_1^2} - K_0 \tilde{\gamma} = -\mu \left(\frac{d\tilde{u}_1}{d\tilde{x}_2} + \frac{d\tilde{u}_2}{d\tilde{x}_1} - \tilde{\gamma} \right) + \tau_0. \quad (\text{A } 7)$$

With the assumption of equation (A 1) for simple shear, equation (2.11) results in

$$0 = \mu \frac{d^2 \tilde{u}_1}{d\tilde{x}_2^2} \quad \text{and} \quad 0 = \mu \left(\frac{d^2 \tilde{u}_2}{d\tilde{x}_1^2} - \frac{d\tilde{\gamma}}{d\tilde{x}_1} \right). \quad (\text{A } 8)$$

Integration results in the displacement fields

$$\tilde{u}_{1A} = k_{uA} \tilde{x}_2 + d_{uA}, \quad \tilde{u}_{1B} = k_{uB} \tilde{x}_2 + d_{uB}, \quad u_{1E} = k_{uE} x_2 + d_{uE} \quad (\text{A } 9)$$

and

$$\tilde{u}_{2A} = \int \tilde{\gamma}_A d\tilde{x}_1 + k_{vA} \tilde{x}_1 + d_{vA}, \quad \tilde{u}_{2B} = \int \tilde{\gamma}_B d\tilde{x}_1 + k_{vB} \tilde{x}_1 + d_{vB}, \quad u_{2E} = k_{vE} x_1 + d_{vE}, \quad (\text{A } 10)$$

where $k_{uA}, k_{uB}, k_{uE}, d_{uA}, d_{uB}, d_{uE}$ and $k_{vA}, k_{vB}, k_{vE}, d_{vA}, d_{vB}, d_{vE}$ are 12 unknown integration constants. With these relations the plastic slip distribution within grain A

$$\tilde{\gamma}_A(\tilde{x}_1) = c_{1A} \exp\left(\sqrt{\frac{K_0}{K_g}} \tilde{x}_1\right) + c_{2A} \exp\left(-\sqrt{\frac{K_0}{K_g}} \tilde{x}_1\right) + \frac{G(k_{uA} + k_{vA}) - \tau_0}{K_0}, \quad (\text{A } 11)$$

and the plastic slip distribution within grain B

$$\tilde{\gamma}_B(\tilde{x}_1) = c_{1B} \exp\left(\sqrt{\frac{K_0}{K_g}} \tilde{x}_1\right) + c_{2B} \exp\left(-\sqrt{\frac{K_0}{K_g}} \tilde{x}_1\right) + \frac{G(k_{uB} + k_{vB}) - \tau_0}{K_0}, \quad (\text{A } 12)$$

result from equation (A 7), with constants $c_{1A}, c_{2A}, c_{1B}, c_{2B}$. In the following, the boundary conditions are introduced to determine the 16 constants.

(c) Boundary conditions

(i) Boundary conditions for plastic slip

At the grain boundaries between an elasto-plastic grain and the elastic grain no plastic deformation occurs. Consequently, the grain boundaries are microhard, i.e.

$$\tilde{\gamma}_A \left(\tilde{x}_1 = -\frac{h_A}{\cos(\vartheta_A)} \right) = 0 \quad \text{and} \quad \tilde{\gamma}_B \left(\tilde{x}_1 = \frac{h_B}{\cos(\vartheta_B)} \right) = 0. \quad (\text{A } 13)$$

At the grain boundary between the two elasto-plastic grains, in general, a discontinuous distribution of the plastic slip is assumed. With the right-hand limit γ_{SB} and a left-hand limit γ_{SA} , the boundary conditions read

$$\tilde{\gamma}_A(\tilde{x}_1 = 0) = \gamma_{SA} \quad \text{and} \quad \tilde{\gamma}_B(\tilde{x}_1 = 0) = \gamma_{SB}. \quad (\text{A } 14)$$

With equations (A 13)–(A 14) four boundary conditions are obtained, which are sufficient to solve for the four constants c_{1A} , c_{2A} , c_{1B} and c_{2B} .

(ii) Boundary conditions for the displacement field

The laminate is exposed to a simple shear deformation. For this case four loading conditions can be determined. At $x_2 = 0$, no displacement occurs, i.e.

$$u_{1A}(x_1, x_2 = 0) = u_{1B}(x_1, x_2 = 0) = u_{1E}(x_1, x_2 = 0) = 0. \quad (\text{A } 15)$$

At $x_2 = 1$, the constant macroscopic shear strain \bar{K} is applied, i.e.

$$u_{1A}(x_1, x_2 = 1) = u_{1B}(x_1, x_2 = 1) = u_{1E}(x_1, x_2 = 1) = \bar{K}. \quad (\text{A } 16)$$

Additionally to the loading conditions, the continuity of the displacement field

$$u_{2A}(x_1 = 0, x_2) = u_{2B}(x_1 = 0, x_2) \quad (\text{A } 17)$$

and

$$u_{2B}(x_1 = h_B, x_2) = u_{2E}(x_1 = h_B, x_2) \quad (\text{A } 18)$$

and the continuity of the stress vector

$$[\sigma n_S] = 0, \quad n_S = e_1, \quad (\text{A } 19)$$

is taken into account. Finally, u_2 is assumed to be a periodic fluctuation field. With the continuity of u_2 at the grain boundaries, the periodicity condition reads

$$\int_{-h_A}^0 \frac{\partial u_{2A}}{\partial x_1} dx_1 + \int_0^{h_B} \frac{\partial u_{2B}}{\partial x_1} dx_1 + \int_{h_B}^{h_B+h_E} \frac{\partial u_{2E}}{\partial x_1} dx_1 = 0. \quad (\text{A } 20)$$

The definition of u_2 as fluctuation requires

$$\int_{-h_A}^0 u_{2A} dx_1 + \int_0^{h_B} u_{2B} dx_1 + \int_{h_B}^{h_B+h_E} u_{2E} dx_1 = 0. \quad (\text{A } 21)$$

With equations (A 15)–(A 21), 12 boundary conditions are obtained, which are sufficient to solve for the 12 integration constants of the displacement fields u_A , u_B and u_E .

References

1. Gurtin ME. 2002 A gradient theory of single-crystal viscoplasticity that accounts for geometrically necessary dislocations. *J. Mech. Phys. Solids* **50**, 5–32. (doi:10.1016/S0022-5096(01)00104-1)
2. Gurtin ME, Needleman A. 2005 Boundary conditions in small-deformation, single-crystal plasticity that account for the Burgers vector. *J. Mech. Phys. Solids* **53**, 1–31. (doi:10.1016/j.jmps.2004.06.006)

3. Soer WA, De Hosson JTM. 2005 Detection of grain-boundary resistance to slip transfer using nanoindentation. *Mater. Lett.* **59**, 3192–3195. (doi:10.1016/j.matlet.2005.03.075)
4. Ohmura T, Tsuzaki K. 2007 Plasticity initiation and subsequent deformation behavior in the vicinity of single grain boundary investigated through nanoindentation technique. *J. Mater. Sci.* **42**, 1728–1732. (doi:10.1007/s10853-006-0885-y)
5. Soer WA, Aifantis KE, De Hosson JTM. 2005 Incipient plasticity during nanoindentation at grain boundaries in body-centered cubic metals. *Acta Mater.* **53**, 4665–4676. (doi:10.1016/j.actamat.2005.07.001)
6. Wang MG, Ngan AHW. 2004 Indentation strain burst phenomenon induced by grain boundaries in niobium. *J. Mater. Res.* **19**, 2478–2486. (doi:10.1557/JMR.2004.0316)
7. Wo PC, Ngan AHW. 2004 Investigation of slip transmission behavior across grain boundaries in polycrystalline Ni3Al using nanoindentation. *J. Mater. Res.* **19**, 189–201. (doi:10.1557/jmr.2004.19.1.189)
8. Kalidindi SR, Vachhani SJ. 2014 Mechanical characterization of grain boundaries using nanoindentation. *Curr. Opin. Solid State Mater. Sci.* **18**, 196–204. (doi:10.1016/j.cossms.2014.05.002)
9. Lagow B, Robertson IM, Jouiad M, Lassila D, Lee TC, Birnbaum H. 2001 Observation of dislocation dynamics in the electron microscope. *Mater. Sci. Eng. A-Struct. Mater. Propert. Microstruct. Process.* **309**, 445–450. (doi:10.1016/S0921-5093(00)01699-3)
10. Kacher J, Robertson IM. 2014 In situ and tomographic analysis of dislocation/grain boundary interactions in α -titanium. *Phil. Mag.* **94**, 814–829. (doi:10.1080/14786435.2013.868942)
11. Clayton JD. 2018 Mesoscale models of interface mechanics in crystalline solids: a review. *J. Mater. Sci.* **53**, 5515–5545. (doi:10.1007/s10853-017-1596-2)
12. Read WT, Shockley W. 1950 Dislocation models of crystal grain boundaries. *Phys. Rev.* **78**, 275–289. (doi:10.1103/PhysRev.78.275)
13. Wolf D. 1989 A read-shockley model for high-angle grain boundaries. *Scr. Metall.* **23**, 1713–1718. (doi:10.1016/0036-9748(89)90348-7)
14. Abrivard G, Busso EP, Forest S, Appolaire B. 2012 Phase field modelling of grain boundary motion driven by curvature and stored energy gradients. Part I: theory and numerical implementation. *Phil. Mag.* **92**, 3618–3642. (doi:10.1080/14786435.2012.713135)
15. Bayerschen E, McBride AT, Reddy BD, Böhlke T. 2016 Review on slip transmission criteria in experiments and crystal plasticity models. *J. Mater. Sci.* **51**, 2243–2258. (doi:10.1007/s10853-015-9553-4)
16. Shi J, Zikry MA. 2011 Modeling of grain boundary transmission, emission, absorption and overall crystalline behavior in $\Sigma 1$, $\Sigma 3$, and $\Sigma 17b$ bicrystals. *J. Mater. Res.* **26**, 1676–1687. (doi:10.1557/jmr.2011.192)
17. Haouala S, Alizadeh R, Bieler TR, Segurado J, LLorca J. 2020 Effect of slip transmission at grain boundaries in Al bicrystals. *Int. J. Plast.* **126**, 102600. (doi:10.1016/j.ijplas.2019.09.006)
18. Spearot DE, Sangid MD. 2014 Insights on slip transmission at grain boundaries from atomistic simulations. *Curr. Opin. Solid State Mater. Sci.* **18**, 188–195. (doi:10.1016/j.cossms.2014.04.001)
19. Liu W, Liu Y, Sui H, Chen L, Yu L, Yi X, Duan H. 2020 Dislocation-grain boundary interaction in metallic materials: Competition between dislocation transmission and dislocation source activation. *J. Mech. Phys. Solids* **145**, 104158. (doi:10.1016/j.jmps.2020.104158)
20. Gurtin ME. 2008 A theory of grain boundaries that accounts automatically for grain misorientation and grain-boundary orientation. *J. Mech. Phys. Solids* **56**, 640–662. (doi:10.1016/j.jmps.2007.05.002)
21. Nye JF. 1953 Some geometrical relations in dislocated crystals. *Acta Metall.* **1**, 153–162. (doi:10.1016/0001-6160(53)90054-6)
22. Peng XL, Huang GY, Bargmann S. 2019 Gradient crystal plasticity: a grain boundary model for slip transmission. *Materials* **12**, 3761. (doi:10.3390/ma1223761)
23. Werner E, Prantl W. 1990 Slip transfer across grain and phase boundaries. *Acta Metall. Mater.* **38**, 533–537. (doi:10.1016/0956-7151(90)90159-E)
24. Hamid M, Lyu H, Schuessler BJ, Wo PC, Zbib HM. 2017 Modeling and characterization of grain boundaries and slip transmission in dislocation density-based crystal plasticity. *Crystals* **7**, 152. (doi:10.3390/cryst7060152)
25. Alipour A, Reese S, Svendsen B, Wulfinghoff S. 2020 A grain boundary model considering the grain misorientation within a geometrically nonlinear gradient-extended crystal viscoplasticity theory. *Proc. R. Soc. A* **476**, 20190581. (doi:10.1098/rspa.2019.0581)

26. Sun S, Adams B, Shet C, Saigal S, King W. 1998 Mesoscale investigation of the deformation field of an aluminum bicrystal. *Scr. Mater.* **39**, 501–508. (doi:10.1016/S1359-6462(98)00189-4)
27. Sedláček R, Forest S. 2000 Non-local plasticity at microscale: a dislocation-based and a Cosserat model. *Phys. Status Solidi (B)* **221**, 583–596.
28. Forest S, Sedláček R. 2003 Plastic slip distribution in two-phase laminate microstructures: dislocation-based versus generalized-continuum approaches. *Phil. Mag.* **83**, 245–276. (doi:10.1080/0141861021000022255)
29. Forest S. 2008 Some links between Cosserat, strain gradient crystal plasticity and the statistical theory of dislocations. *Phil. Mag.* **88**, 3549–3563. (doi:10.1080/14786430802154815)
30. Cordero NM, Gaubert A, Forest S, Busso EP, Gallerneau F, Kruch S. 2010 Size effects in generalised continuum crystal plasticity for two-phase laminates. *J. Mech. Phys. Solids* **58**, 1963–1994. (doi:10.1016/j.jmps.2010.06.012)
31. Aslan O, Cordero NM, Gaubert A, Forest S. 2011 Micromorphic approach to single crystal plasticity and damage. *Int. J. Eng. Sci.* **49**, 1311–1325. (doi:10.1016/j.ijengsci.2011.03.008)
32. Forest S, Guéninchault N. 2013 Inspection of free energy functions in gradient crystal plasticity. *Acta Mech. Sin.* **29**, 763–772. (doi:10.1007/s10409-013-0088-0)
33. Wulfinghoff S, Forest S, Böhlke T. 2015 Strain gradient plasticity modeling of the cyclic behavior of laminate microstructures. *J. Mech. Phys. Solids* **79**, 1–20. (doi:10.1016/j.jmps.2015.02.008)
34. Erdle H, Böhlke T. 2017 A gradient crystal plasticity theory for large deformations with a discontinuous accumulated plastic slip. *Comput. Mech.* **60**, 923–942. (doi:10.1007/s00466-017-1447-7)
35. Prahs A, Böhlke T. 2020 On interface conditions on a material singular surface. *Contin. Mech. Thermodyn.* **32**, 1417–1434. (doi:10.1007/s00161-019-00856-1)
36. Mecking H, Lücke K. 1970 A new aspect of the theory of flow stress of metals. *Scr. Metall.* **4**, 427–432. (doi:10.1016/0036-9748(70)90078-5)
37. Kocks F, Mecking H. 2003 Physics and phenomenology of strain hardening: The FCC case. *Prog. Mater. Sci.* **48**, 171–273. (doi:10.1016/S0079-6425(02)00003-8)
38. Le KC. 2018 Thermodynamic dislocation theory for non-uniform plastic deformations. *J. Mech. Phys. Solids* **111**, 157–169. (doi:10.1016/j.jmps.2017.10.022)
39. Piao Y, Le KC. 2022 Thermodynamic theory of dislocation/grain boundary interaction. *Contin. Mech. Thermodyn.* **34**, 763–780. (doi:10.1007/s00161-022-01088-6)
40. Cermelli P, Gurtin ME. 2002 Geometrically necessary dislocations in viscoplastic single crystals and bicrystals undergoing small deformations. *Int. J. Solids Struct.* **39**, 6281–6309. (doi:10.1016/S0020-7683(02)00491-2)
41. Gurtin ME, Fried E, Anand L. 2010 *The mechanics and thermodynamics of continua*. Cambridge, UK: Cambridge University Press.
42. Maugin GA. 1993 *Material inhomogeneities in elasticity*, 1st edn. London, UK: Chapman and Hall.
43. Truesdell C, Toupin R. 1960 In *The Classical Field Theories* (ed. S Flügge), pp. 226–858. Berlin, Heidelberg: Springer.
44. Bayerschen E, Böhlke T. 2016 Power-law defect energy in a single-crystal gradient plasticity framework: a computational study. *Comput. Mech.* **58**, 13–27. (doi:10.1007/s00466-016-1279-x)
45. Bargmann S, Reddy BD. 2011 Modeling of polycrystals using a gradient crystal plasticity theory that includes dissipative micro-stresses. *Eur. J. Mech. A. Solids* **30**, 719–730. (doi:10.1016/j.euromechsol.2011.04.006)
46. Prahs A, Böhlke T. 2022 The role of dissipation regarding the concept of purely mechanical theories in plasticity. *Mech. Res. Commun.* **119**, 103832. (doi:10.1016/j.mechrescom.2021.103832)
47. Simo JC, Hughes TJR. 1998 *Computational inelasticity*. Interdisciplinary Applied Mathematics, 7. New York, NY: Springer.
48. Müller I. 1985 *Thermodynamics*. Interaction of Mechanics and Mathematics Series. Boston, MA: Pitman.
49. Peng XL, Husser E, Huang GY, Bargmann S. 2018 Modeling of surface effects in crystalline materials within the framework of gradient crystal plasticity. *J. Mech. Phys. Solids* **112**, 508–522. (doi:10.1016/j.jmps.2018.01.007)
50. Özdemir İ, Yalçinkaya T. 2014 Modeling of dislocation-grain boundary interactions in a strain gradient crystal plasticity framework. *Comput. Mech.* **54**, 255–268. (doi:10.1007/s00466-014-0982-8)

51. Gottschalk D, McBride A, Reddy BD, Javili A, Wriggers P, Hirschberger CB. 2016 Computational and theoretical aspects of a grain-boundary model that accounts for grain misorientation and grain-boundary orientation. *Comput. Mater. Sci.* **111**, 443–459. (doi:10.1016/j.commatsci.2015.09.048)
52. McBride A, Bargmann S, Reddy BD. 2015 A computational investigation of a model of single-crystal gradient thermoplasticity that accounts for the stored energy of cold work and thermal annealing. *Comput. Mech.* **55**, 755–769. (doi:10.1007/s00466-015-1134-5)
53. Reddy BD. 2011 The role of dissipation and defect energy in variational formulations of problems in strain-gradient plasticity. Part 2: single-crystal plasticity. *Continu. Mech. Thermodyn.* **23**, 551. (doi:10.1007/s00161-011-0195-8)
54. Beyerlein IJ *et al.* 2012 Structure–property–functionality of bimetal interfaces. *JOM* **64**, 1192–1207. (doi:10.1007/s11837-012-0431-0)
55. Bayerschen E, Stricker M, Wulfinghoff S, Weygand D, Böhlke T. 2015 Equivalent plastic strain gradient plasticity with grain boundary hardening and comparison to discrete dislocation dynamics. *Proc. R. Soc. A* **471**, 20150388. (doi:10.1098/rspa.2015.0388)
56. Duda FP, Šilhavý M. 2004 Dislocation walls in crystals under single slip. *Comput. Methods Appl. Mech. Eng.* **193**, 5385–5409. (doi:10.1016/j.cma.2003.12.069)
57. Erdle H, Böhlke T. 2023 Analytical investigation of a grain boundary model that accounts for slip system coupling in gradient crystal plasticity frameworks. Figshare. (doi:10.6084/m9.figshare.c.6631533)